JOURNAL OF MATERIALS SCIENCE 20 (1985) 274–288

The mechanisms of yield and plastic flow in HgTe and $Cd_xHg_{1-x}Te$

S. COLE*, A. F. W. WILLOUGHBY, M. BROWN‡
Engineering Materials Department, Southampton University, Southampton, UK

Single crystals of HgTe and $Cd_xHg_{1-x}Te$ ($0.18 < x < 0.30$), oriented for single slip, have been deformed in four-point bending at strain rates $\sim 10^{-4}$ sec^{-1} and temperatures from −11 to + 84° C for HgTe, and 20 to 195° C for $Cd_xHg_{1-x}Te$. At the lowest temperatures, the stress–strain curve exhibits a sharp yield relaxation and subsequent zero work hardening regime, as commonly observed for other semiconductors. Experiments show that the yielding mechanism is that proposed by Johnston and Gilman for LiF. Possible explanations for the post-yield zero work hardening phenomenon are discussed. The influence of composition, temperature and strain rate on the stress–strain behaviour are reported. At 20° C, the upper and lower yield stresses (τ_{uy} and τ_{ly}) increase with increasing x in qualitative agreement with our earlier hardness results. For $Cd_{0.2}Hg_{0.8}Te$, τ_{ly} varies with temperature, T, at a strain rate of 10^{-4} sec^{-1}, according to $\tau_{ly} \propto \exp(Q/kT)$ where Q is 0.16 eV. For HgTe the comparable value is 0.11 eV. At $x = 0.25$ and constant temperature, τ_{ly} depends on strain rate γ as $\tau_{ly} \propto \gamma^{1/n}$ where n is 4. The stress level for deformation of $Cd_{0.2}Hg_{0.8}Te$ at $\gamma \sim 10^{-4}$ sec^{-1} and 20° C is 2–3 kg mm^{-2}, comparable with that for InSb at 300° C or Si at 1000° C. Strain rate cycling tests on $Cd_xHg_{1-x}Te$ give values of activation volume V^* around $10\,b^3$ at 20° C, independent of plastic strain (up to 2–3%), suggesting that deformation in these alloys is controlled by the Peierls mechanism, as observed in other II–VI compounds.

1. Introduction

The ternary alloys $Cd_xHg_{1-x}Te$ (CMT) are of considerable importance as materials for infrared detectors. Problems associated with the crystal growth and processing of these materials have highlighted the necessity for an understanding of their basic properties, including their mechanical behaviour.

CMT may be regarded as a pseudo-binary alloy of the parent binary compounds CdTe and HgTe. While a number of authors have made detailed mechanical measurements on CdTe (Hall and Van der Sande [1], Maeda *et al.* [2] and Gutmanas *et al.* [3]), work on HgTe and the ternary alloy is sparse, and is based predominantly on hardness measurements [4, 5]. The present project was instigated to obtain reliable data on the bulk mechanical behaviour of CMT.

In earlier papers we have reported results on the shape of the stress–strain curve and the temperature dependence of the yield stress in three-point bending [6] and the variation of the mechanical properties with composition across the pseudo-binary section using the microhardness test [7]. However, constraints imposed by the available material made control of composition and crystallographic orientation of the samples less than ideal.

In the present study, attempts are made, as described later to eliminate these uncontrolled variables. Four-point bending is used, this being less sensitive to inhomogeneities in the test-piece

*Present address: British Telecom Research Laboratories, Martlesham Heath, Ipswich, IP5 7RE, UK.
‡Present address: Rockwell International Science Center, Thousand Oaks, California 91360, U.S.A.

0022–2461/85 $03.00 + .12

than is the three-point technique. Preliminary data on the variation of the yield stress with composition and temperature have already been published [8]. This paper discusses these results more fully and in the light of new detailed measurements on the strain rate dependence of the yield stress.

Much interest in recent years has centred around the plastic deformation process in the II–VI compounds, in an attempt to throw light on the nature of various unusual phenomena, such as the photoplastic effect, exhibited by these materials [9]. It is the aim of this paper to provide insight into the mechanisms of yield and plastic flow in CMT.

2. Experimental procedures

2.1. Sample preparation

HgTe slices, 1 mm thick, cut on {1 1 1} orientation from single crystals grown by the travelling heater method were obtained from CNRS, Meudon, France. CMT was provided by Mullard Southampton, England, in the form of slices, 12 mm diameter and 0.5 mm thick, cut perpendicular to the growth axis from an ingot grown by the Bridgman method.

After cleaning in hot methanol to remove wax, the slices were chemically polished in 5 vol % bromine in methanol (Br/Meoh) to remove surface cutting damage, and etched in Polisar etch 2(12 cm^3 HNO_3, 5 cm^3 HCl, 1 cm^3 glacial CH_3COOH, 18 cm^3 H_2O, 0.02 cm^3 Br_2; Polisar *et al.* [11]). This etchant, developed originally for HgTe, is a dislocation etchant for CMT [12], and produces pits on the (1 1 1) *A* face [13], leaving the $(\bar{1}\bar{1}\bar{1})$ *B* face oxidized. Similar behaviour is observed for HgTe [11]. The etch therefore both revealed structural defects and provided a means of identification of the absolute crystallographic polarity of the crystals.

In both HgTe and CMT, major grain boundaries (where present) sub-grain boundaries and individual dislocations were revealed. The HgTe slices were all single crystal and had a total etch pit density of 2×10^6 cm^{-2}, with about two-thirds of the pits lying in sub-grain boundaries, the sub-grain diameter being 50 to 200 μm. The CMT slices were predominantly single crystal, having only small secondary grains. The crystallographic orientation of the surface plane, established for each slice by means of a Laue back-reflection X-ray photograph, was as shown in Fig. 1. The substructure was similar to that of the HgTe samples, with a total

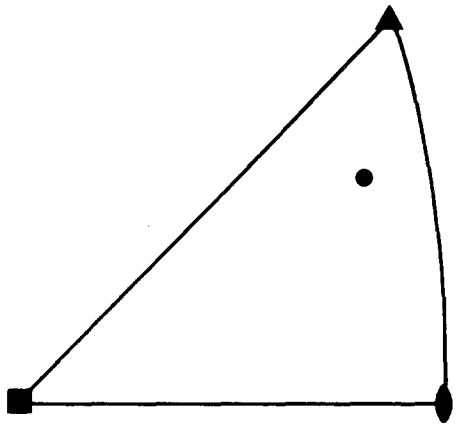

Figure 1 Crystallographic orientation of the surface plane of the CMT slices.

etch-pit density of about 2×10^6 cm^{-2}, mostly within sub-grain walls, and a sub-grain size of 30 to 150 μm (Fig. 2).

The segregation in the CdTe–HgTe pseudo-binary system gives rise to considerable longitudinal composition gradients in the directionally solidified Bridgman ingots [14], so that the mean compositions of adjacent slices differ. In addition, each slice exhibits radial variations in composition. In this work, attention was confined to slices having mean compositions in the range $0.18 \leqslant x \leqslant 0.30$, in which the radial variations are less than ± 0.01 in x [14]. The compositions of a number of slices have been measured by infrared transmission (using the bandgap/composition relationship due to Schmit [15]) so that the composition of every slice could be inferred by interpolation.

In order to produce slip on a single slip system, it was considered desirable for the samples to have a long axis of ⟨1 2 3⟩. Such directions lie in the surface plane of both the HgTe and the CMT

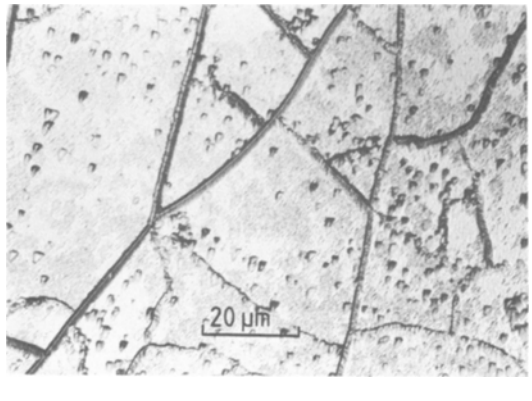

Figure 2 Dislocation substructure of undeformed CMT as revealed by 25 secs etch using Polisar etch 2.

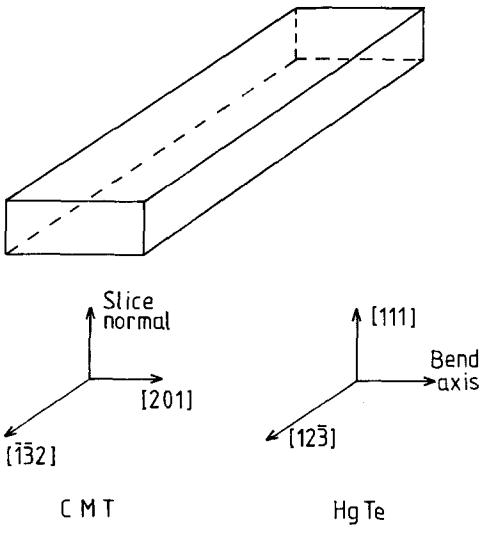

Figure 3 Geometry of HgTe and CMT bend test samples.

slices. Therefore, with the aid of a Laue back-reflection X-ray photograph, bend test-pieces having dimensions 12 mm x 3 mm x 0.5 mm (12 mm x 3 mm x 1 mm for HgTe) with a ⟨123⟩ long axis, were cut from the slices using a diamond saw. They were chemically polished in 5 vol% Br/MeOH to remove both the cutting damage from their edges and the original etching features. Appropriate masking with chemically resistant lacquer was used to preserve the rectangular cross-section. Fig. 3 shows the sample geometries.

2.2. Bend-jig design

The tests were conducted using the jig shown in Fig. 4. The sample is deformed between four Spectrosil quartz knife edges and the remainder of the jig is of stainless steel. It is designed so that the upper and lower knife edges can pivot independently on orthogonal axes to permit even settling on a dimensionally uneven sample. The whole jig fits in the compression cage of a model TM-M-L Instron machine, fitted with a type 2511-102 2 kg load cell. The compression cage could be surrounded by either a liquid bath or an electric resistance furnace, as required.

2.3. Bend tests

In this section only the general features of the tests are described. Details are discussed later.

Tests on HgTe were conducted at a glide strain rate of the order of 10^{-4} sec^{-1} and temperatures in the range −11 to +84° C. The lower temperatures were achieved using a cooled methanol bath, while for those above room temperature a heated

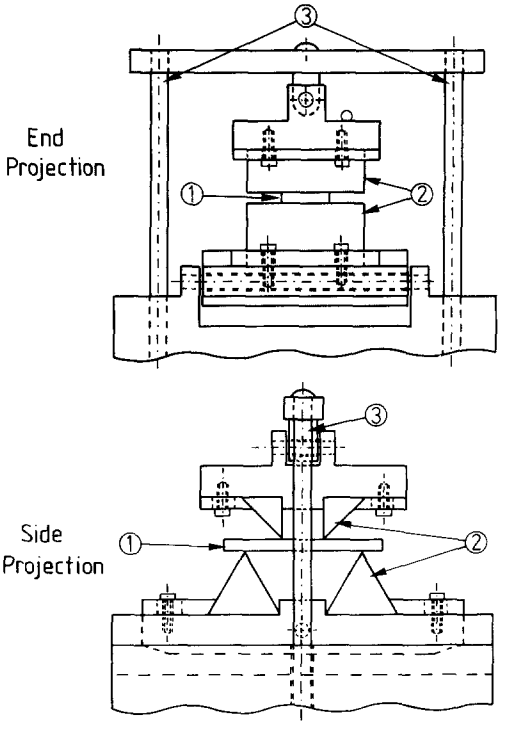

Figure 4 Design of the four-point bend jig. 1. Test piece; 2. Quartz knife edges; 3. Silver steel guide rods. Other parts stainless steel.

deionized water bath was employed. Thermal insulation of these baths maintained a stable temperature within ± 1° C for the period of any test, temperatures being measured using a thermometer close to the sample.

CMT samples were tested in air at strain rates between 1.2×10^{-4} sec^{-1} and 6×10^{-3} sec^{-1} and temperatures from 20 to 195° C, using an electric resistance furnace around the compression cage. Temperatures were monitored within 1 cm of the test-piece with the aid of a chromel/alumel thermocouple.

As described in [8], the stress (τ) and strain (γ) were derived from the load on the sample and its bending deflection using the relations of Bruneau and Pratt [16].

3. Results and discussion

3.1. HgTe

Test-pieces of HgTe with ⟨123⟩ orientation were bent at an outer fibre glide strain rate of 2.5×10^{-4} sec^{-1} and temperatures in the range −11 to +84° C. Samples were bent in pairs at similar temperatures but in opposite crystallographic senses (i.e. with the (111) Hg face concave or convex) to test for any difference in the stress-

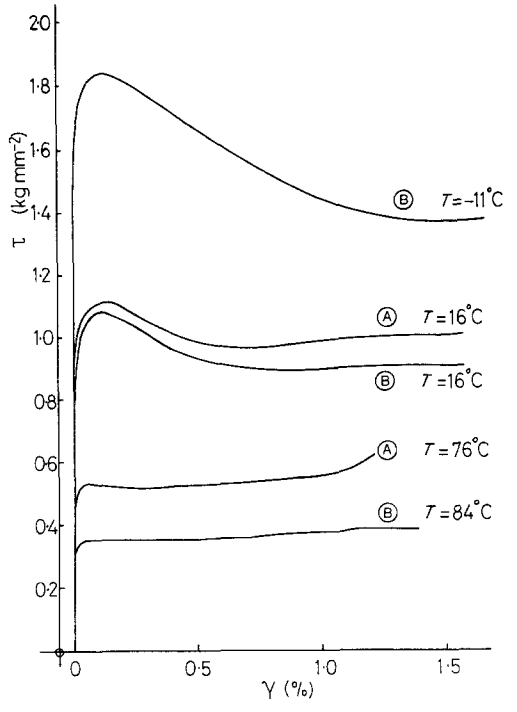

Figure 5 Stress–strain curves for ⟨1 2 3⟩ HgTe samples deformed at a strain rate of 2.5×10^{-4} sec^{-1}.

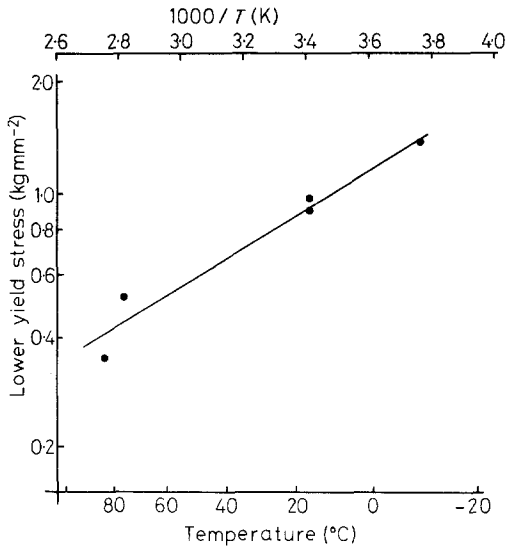

Figure 6 Lower yield stresses (log scale) versus temperature (reciprocal K) for HgTe.

strain characteristics. This would introduce an excess of 60° *A* (glide) dislocations on all the possible slip planes when the Hg face is concave, and 60° *B* (glide) dislocations when the Hg face is convex.

The $\tau-\gamma$ curves obtained for these samples are shown in Fig. 5. It is clear that, at the lowest temperature, the curve shows a marked yield relaxation. As the temperature is raised, the magnitude of this yield relaxation (i.e. the area under the stress–strain curve in the yield region above the lower yield stress) diminishes, and it is not observed at all at 84° C. In all tests the stress after yield was fairly constant up to 1 or 2% strain. At 16° C (close to room temperature) the yield stress is around 1 kg mm^{-2}, similar to that for pure Pb [17].

There appears to be no significant difference between the curves for samples bent in opposite crystallographic senses. This indicates that in both cases the same type of dislocation is controlling the rate of glide. This is consistent with the results of Sumino and Shimizu [18] on InSb, who showed that the screw segments of the expanding dislocation loops are rate controlling.

The lower yield stresses (τ_{1y}) measured from these curves are plotted on a log scale as a function of reciprocal temperature (T) in Fig. 6. The linear behaviour suggests that $\tau_{1y} \alpha \exp(Q/kT)$ where the activation energy Q may be estimated from the slope of the line to be 0.11 eV. This relationship is commonly observed in semiconductors [19].

3.2. CMT

In all cases, tests on CMT were conducted with the originally etched face (close to (1 1 1) Cd, Hg) concave. This means that all possible slip planes were in *A* (glide) bending.

3.2.1. Form of the stress–strain curve and its composition dependence

Samples of various compositions between $x = 0.18$ and 0.30 were tested under similar conditions of temperature and strain rate. Two series of tests were conducted, using a strain rate of 1.25×10^{-4} sec^{-1}, one at 20° C, the other at 140° C.

The $\tau-\gamma$ curves obtained at 20° C are shown in Fig. 7. They exhibit a marked yield relaxation followed by a zero work hardening regime, similar to the behaviour observed for HgTe in the previous section, and for CMT in three-point bending [6]. This type of curve has been observed commonly for other semiconductors [20–22] and alkali halides [23].

At constant temperature the shape of the curves is independent of the composition. This suggests that the diminution of the yield relaxation with increasing temperature observed for HgTe is a real effect, and is not an artefact of the machine

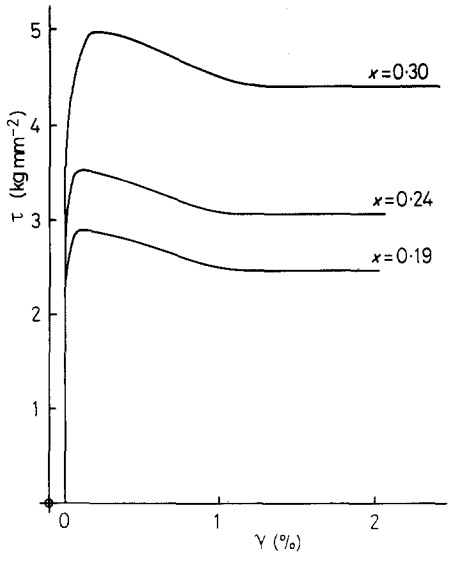

Figure 7 Stress–strain curves for ⟨123⟩ CMT samples of various compositions measured at $T = 20°$ C, $\dot{\gamma} = 1.2 \times 10^{-4}$ sec^{-1}.

insensitivity at low stresses. However, the overall stress level increases with increasing CdTe content (x value). This is shown more clearly in Fig. 8, where the measured upper and lower yield stresses are plotted as a function of x, values for HgTe at 16° C also being included. The results show strong qualitative agreement with the trends observed in

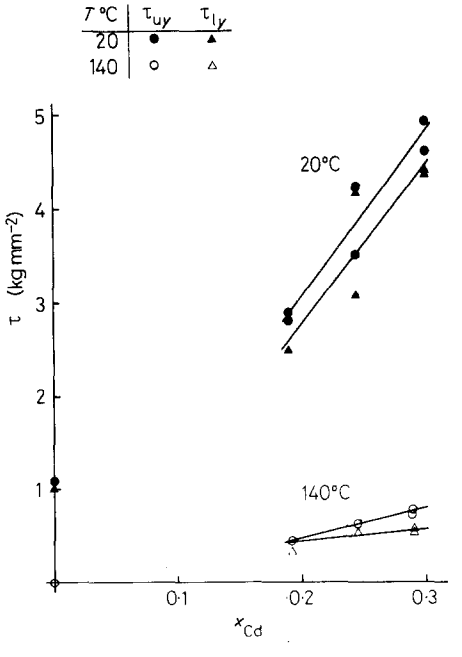

Figure 8 Composition dependence of the upper and lower yield stresses (τ_{uy} and τ_{ly}) for CMT at $\dot{\gamma} = 1.25 \times 10^{-4}$ sec^{-1}.

the room temperature hardness versus composition data obtained by the present authors in [7]. In that paper it was shown how the results could be explained in terms of solid solution hardening, regarding HgTe as the solvent lattice and CdTe as the solute. In particular, the hardening efficiency, dH_v/dx, was found to change fairly abruptly from 40 kg mm^{-2} mol^{-1} for x below 0.2 to 110 kg mm^{-2} mol^{-1} at higher x values. This was attributed to a change in the dislocation/solute interaction mechanism from elastic alone to elastic plus electrical as x increased past 0.2, resulting from the increasing band gap. The present results suggest that the yield stress hardening efficiency, $d\tau_y/dx$ behaves in a similar manner. The maximum possible value of $d\tau/dx$ below $x = 0.2$ is given by the slope of the line between the data for HgTe and $x = 0.2$, which is $d\tau/dx =$ 11 kg mm^{-2} mol^{-1}. Above $x = 0.2$ this rises to 17 kg mm^{-2} mol^{-1}.

Mott and Nabarro [24] obtained an approximate formula for the increment of the yield stress due to solute, $\Delta\tau$:

$$\Delta\tau = G\epsilon^2 x$$

Where G is the shear modulus of the matrix, ϵ the misfit parameter of the solute atoms. Hence

$$\frac{d\tau}{dx} = G\epsilon^2$$

For CMT, a rough estimate of the total elastic misfit gives, for screw dislocations (which are rate controlling) [7] $\epsilon = 4 \times 10^{-2}$. Taking G for HgTe as 20.5 GNm^{-2} [7] we obtain $d\tau/dx = 3.3$ kg mm^{-2} mol^{-1}, considering elastic solute/dislocation interactions alone. Bearing in mind that the experimental value of $d\tau/dx$ below $x = 0.2$ of 11 kg mm^{-2} mol^{-1} is an upper limit, and also the approximate nature of the calculations, the agreement is remarkable. This suggests that the hardening in the low x region may be attributed to elastic dislocation/solute interactions, as tentatively proposed in [7].

3.2.2. Temperature dependence of the stress–strain behaviour

Samples of CMT having compositions in the range $0.18 < x < 0.30$ were deformed at a strain rate of 1.25×10^{-4} sec^{-1} and temperatures in the range 20 to 195° C. Even at the highest temperatures, no visible surface degradation was observed.

Typical stress–strain curves for CMT having

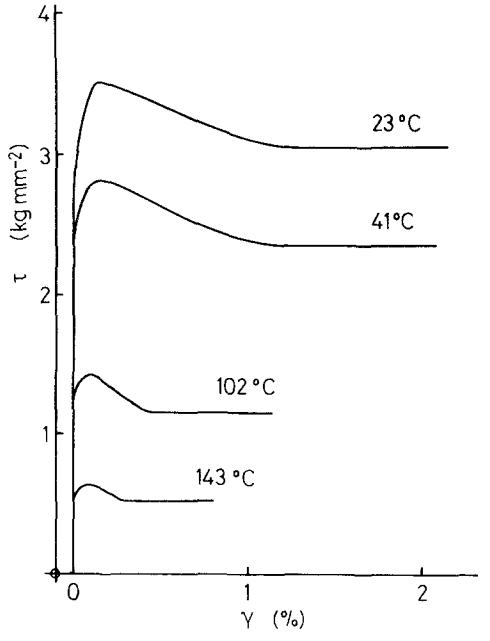

Figure 9 Stress–strain curves for ⟨1 2 3⟩ CMT samples deformed in bending at various temperatures ($\dot{\gamma} = 1.25 \times 10^{-4}$ sec^{-1}, x = 0.26).

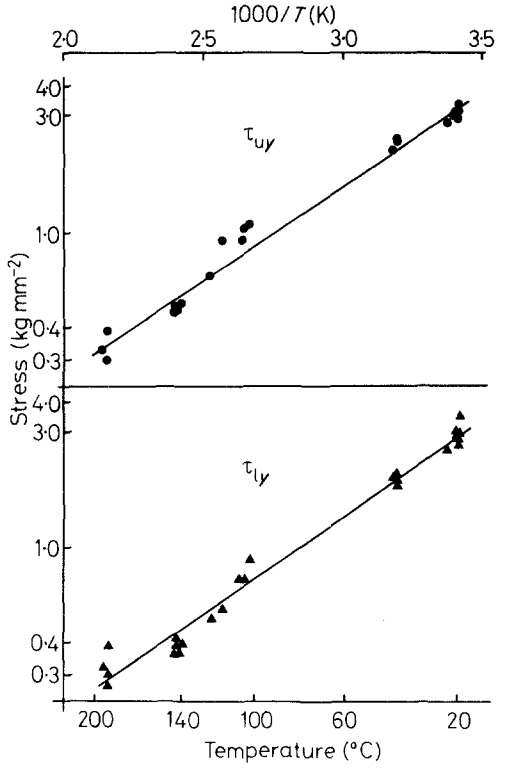

Figure 10 Log τ_{uy}, log τ_{1y} plotted against 1000/T(K). Stresses normalized to $x = 0.2$, $\dot{\gamma} = 1.27 \times 10^{-4}$ sec^{-1}.

$x = 0.26$ are shown in Fig. 9. The curves show similar trends to those observed for HgTe; that is:

1. At lower temperatures there is a marked yield relaxation, the magnitude of which diminishes as temperature increases. Unlike HgTe, however, the yield point for CMT is still present even at the highest temperature, where the stress level is about 0.5 kg mm^{-2}. At this stress level, no yield point was detected for HgTe.

2. The general stress level for deformation of CMT decreases rapidly with increasing temperature. In order to quantify the temperature dependence of the yield stresses for CMT, it was necessary to correct for the differences in composition between the samples, as described by the present authors in [8]. This was achieved by making a linear interpolation between the yield stress/composition data of Fig. 8, in the range $0.18 < x < 0.30$. Upper and lower yield stresses were hence normalized to a composition of $x = 0.20$, this being one of technological interest.

The normalized yield stress data are plotted on a logarithmic scale as a function of reciprocal absolute temperature in Fig. 10. The linear behaviour indicates that the yield stresses obey a relation of the form $\tau_y \propto \exp(Q/kT)$. The activation energy, Q is calculated as 0.15 eV for τ_{uy} and 0.16 for τ_{1y}. This latter value is consistent with the value of 0.11 eV obtained earlier from the lower yield stress data for HgTe, since HgTe is more readily deformed than is CMT. Comparable values are 0.1 eV measured for $Cd_{0.2}Hg_{0.8}Te$ in three-point bending by Cole [6] and 0.3 eV determined by Kurilo *et al.* [4] from hardness measurements on $Cd_{0.15}Hg_{0.85}Te$. The present result is likely to be the most reliable, for reasons discussed in [8].

3.2.3. Strain rate dependence of the lower yield stress

A number of CMT samples having $x \cong 0.25$ were deformed at the same temperature (in the range 41 to 192° C) at a strain rate, $\dot{\gamma}_1 = 1.25 \times 10^{-4}$ sec^{-1}, until the lower yield point was reached. When flow in the post-yield zero work hardening region was established, the strain rate was changed to a higher value, $\dot{\gamma}_2$ (up to a maximum of 6×10^{-3} sec^{-1}) and the new flow stress measured. Finally, the strain rate was changed back to $\dot{\gamma}_1$ to check that the flow stress was unaltered from the original (that is, that the zero work hardening region had not been exceeded). Hence, information on the flow stress (τ_f) at two different

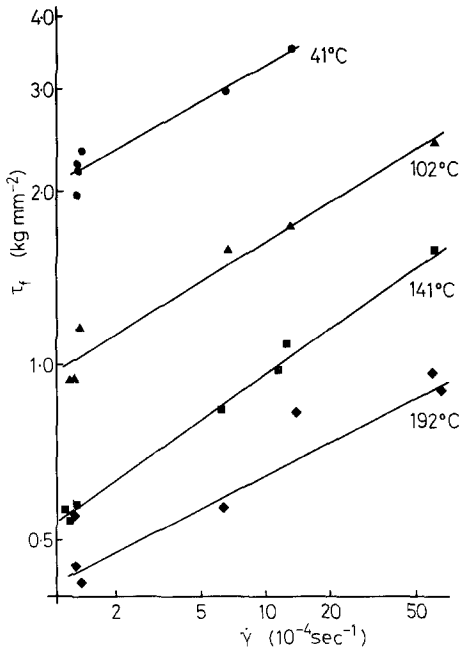

Figure 11 Post yield flow stress for ⟨1 2 3⟩ CMT ($x \sim 0.25$) against strain rate at various temperatures.

strain rates was obtained on a single sample; furthermore, use of the same base strain rate $\dot{\gamma}_1$ for every test provided a check on reproducibility between different samples.

Values of the measured flow stress at four different temperatures are plotted on a logarithmic scale as a function of log $\dot{\gamma}$ in Fig. 11. At each temperature, reasonable fit to a straight line is obtained, giving $\tau_f \propto \dot{\gamma}^{1/n}$. The values of n calculated from the results are listed in Table I. In view of the small number of data points, the variation of n apparent in the table is probably not significant, and therefore we take n as about 4 for CMT ($x \cong 0.25$).

Considering the form of the stress–strain curve (Fig. 7) it is clear that, within the post-yield zero work-hardening region, τ_f is equal to τ_{1y}. In several tests, the strain rate was repeatedly altered between $\dot{\gamma}_1$ and a higher $\dot{\gamma}_2$ and the flow stress at each strain rate was found to be independent of strain within the zero work hardening region, even after a number of cycles. It is suggested, then, that in this sense τ_f is indistinguishable from τ_{1y}, and the observed strain rate independence of τ_f is equivalent to that of τ_{1y}. Hence we may say that $\tau_{1y} \propto \dot{\gamma}^{1/4}$ for CMT ($x \cong 0.25$).

TABLE I Values of n calculated from the flow stress/strain rate data for CMT

Temperature, T(° C)	Composition, x (mean)	n
41	0.23	4.8
102	0.25	4.3
141	0.29	3.8
192	0.28	5.2

3.2.4. Summary

Combining the results of Sections 3.2.2 and 3.2.3, we obtain, for CMT ($x \sim 0.2$):

$$\tau_{1y} \propto \dot{\gamma}^{1/4} \exp[0.16\,(\text{eV})/kT] \qquad (1)$$

From dislocation velocity measurements it is known that, in semiconductor crystals, the velocity of individual dislocations, v is related to the stress, τ and temperature T by

$$v \propto \tau^m$$

$$v \propto \exp(-E/kT)$$

where m is the velocity–stress exponent and E is an activation energy.

Haasen [25] has developed a theory of the yield point in semiconductors, taking into account dislocation multiplication and interaction. He showed that the bulk plastic flow parameters n and Q are related to m and E by

$$x = m + 2$$

$$Q = E/n$$

Hence, we obtain, for CMT, $m \cong 2$ and $E \cong 0.6$ eV. Therefore, it follows that we predict:

$$v \propto \tau^2 \exp[-0.6\,(\text{eV})/kT] \qquad (2)$$

In Section 3.1 it was suggested that screw dislocations are the rate controlling dislocations in the deformation of HgTe. It seems reasonable to assume that this would also be the case for CMT, so Equation 2 describes the motion of screw dislocations in CMT ($x \cong 0.2$).

There is no comparable data for CMT in the literature. In compression tests on ⟨1 1 0⟩ oriented CdTe single crystals, Carlsson and Ahlquist [26] found, using Haasen's theory, $E =$ 0.6 eV, which is identical to the present result for CMT. Measurements of m are rather inconsistent. Carlsson and Ahlquist obtained a value of 9.8 using strain rate cycling, which is clearly appreciably higher than the present result. Gutmanas *et al.* [3] compressed both polycrystals and ⟨1 1 1⟩ oriented single crystals of CdTe and found $m = 10$–12 from strain rate cycling tests. However,

using a "pulse loading" technique, which imposes only a small plastic strain, they found $m = 3$–5. In order to understand these apparent inconsistences, it is necessary to remember that, in such measurements, it is particularly important to minimise changes in the dislocation structure of the crystal [27]. In the present work, this is achieved since all the measurements were made at low strains ($\gamma < 2\%$) on samples in a single slip orientation. On the other hand, both Gutmanas *et al.* and Carlsson and Ahlquist conducted their tests at up to 10% plastic strain on samples not oriented for single slip. They would therefore be in a work-hardening state, the internal structure changing rapidly with strain. This effect would be minimised in the pulse loading tests and it is interesting that the values of m obtained from this method are close to that observed for CMT in this work.

3.3. The yielding mechanism in CMT

This section describes experiments which investigate the nature of the yield point in CMT.

3.3.1. Reloading experiments

A number of samples were deformed into the post-yield zero work hardening region at 120° C and a strain rate of 1.25×10^{-4} sec^{-1}, unloaded, then immediately retested under the original conditions. The resulting behaviour is shown in Fig. 12. On reloading, plastic flow began at the original flow stress, with no reappearance of the yield relaxation. This implies that the yield process changes the internal structure of the sample in some dramatic way, and that the new structure is not significantly altered on removal of the load.

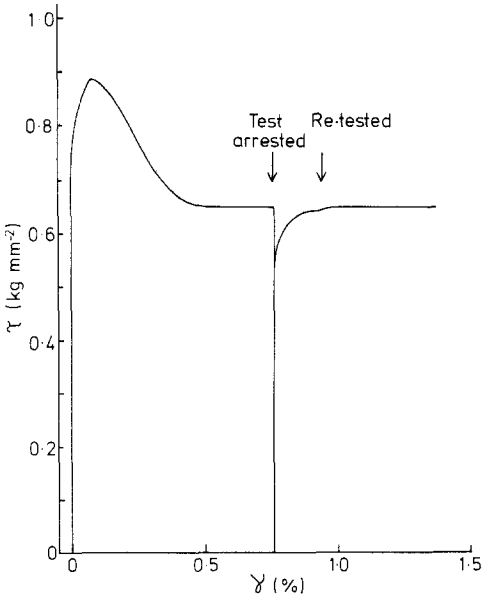

Figure 12 Stress–strain curve for CMT ($x = 0.26$) during unloading/immediate reload cycle. $T = 120°$ C, $\dot{\gamma} = 1.25 \times 10^{-4}$ sec^{-1}.

3.3.2. Observations on the change in dislocation density during yield

To investigate the change in internal structure during yield, a number of samples of similar composition ($x \cong 0.25$) were deformed at 120° C and a strain rate of 1.25×10^{-4} sec^{-1} to various stages in the stress–strain curve, whereupon they were unloaded and cooled to room temperature. Each sample was examined on all faces by optical microscopy for evidence of slip steps; however, except in limited regions close to the points of contact of the knife edges, where multiple slip occurred, they were very difficult to resolve. Accordingly, after a 10 sec polish in 2 vol% Br/MeOH to prepare the surface, each sample was etched in Polisar etch 2 (described earlier) to reveal dislocation etch pits.

Fig. 13 shows optical micrographs of etch pits on the concave face at the recorded upper and lower yield points.

At the upper yield point the total density of etch pits has risen from 1 to 2×10^6 cm^{-2} for the virgin crystal to around 3×10^6 cm^{-2}. Careful inspection reveals that the original network of grown-in dislocations is still present. This may mean that they are sessile, but they may act as sources for fresh, mobile, dislocations during these early stages of deformation. The fresh etch pits lie in lines, parallel to the trace of the expected primary slip plane. Some evidence of slip on a secondary system is observed. The pits appear to lie in distinct bands, within which the etch pit density is about 1 to 2×10^7 cm^{-2}, an order of magnitude higher than the mean density. These bands resemble the Lüders bands observed in plastic deformation of steel, and which have also been seen in other semiconductors [19].

At the lower yield point, the overall pit density has reached 3×10^7 cm^{-2}, and while remants of the original substructure of the undeformed crystal are still retained, there is no evidence of slip bands. The fact that the overall etch pit density at this stage is similar to that within the slip bands at the upper yield point suggests that these bands have spread laterally, with little internal multiplication, gradually filling the gauge

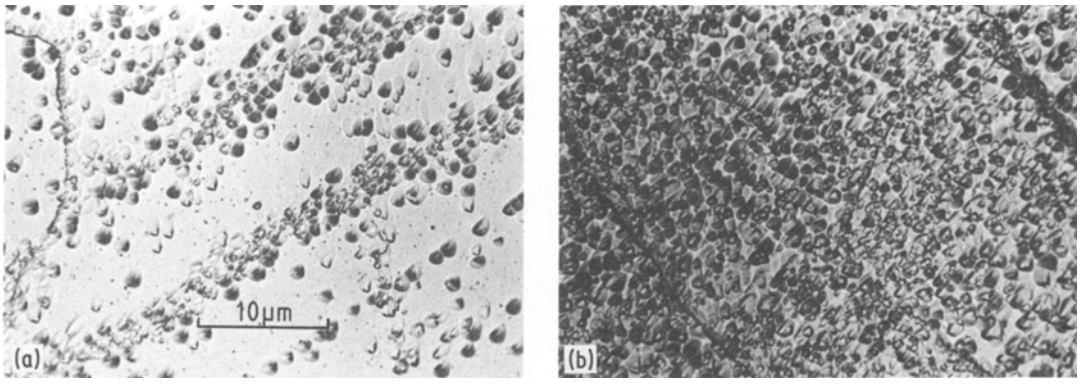

Figure 13 Etch pit distribution on concave surface of ⟨1 2 3⟩ oriented CMT single crystal deformed in bending to (a) the upper yield point (b) the lower yield point at $T = 120°$ C, $\dot{\gamma} = 1.25 \times 10^{-4}$ sec^{-1}. Etched 25 sec. Polisar etch 2.

length by the lower yield point. This is in agreement with the results of Bell and Bonfield [21] for tensile testing of Ge. However, according to Alexander and Haasen [19], this gradual broadening of the slip bands occurs after the lower yield point. They say that it occurs at constant stress and therefore explains the existence of the zero work hardening region following the yield relaxation.

In order to understand the present results, it is necessary to consider the details of the bend test. The stress distribution in an elastically bent beam varies from zero at the neutral plane to a maximum at the outer fibre. Therefore, plastic yield will occur first at the outer fibre, when the stress there reaches τ_{uy}. As bending continues, the yielding region propagates in towards the neutral plane. Behind this "yield front" the material relaxes to the flow regime, continuously deforming at a stress below τ_{uy}. Since the measured stress–strain curve represents an average for the sample, it is clear that this will lag the true behaviour at the outer fibre. The etching results, on the other hand, reveal only the dislocation structure at the outer fibre. Hence, the structure observed at the measured upper yield point, for example, may in fact represent that zero work hardening region. In this event the present results would be more in agreement with those of Alexander and Haasen than with those of Bell and Bonfield. With these considerations, and noting also that the pit density may underestimate the true dislocation density (even if the Polisar etch 2 gives a 1:1 correspondence of pits with dislocations, which has yet to be established) it is clear that we are in no position to make any precise statement about the dislocation density after yield. However, it is clear that it does increase markedly. Furthermore, the results indicate that the original ingrown dislocations appear to be sessile, and may act as sources for fresh dislocations. This latter point explains the difficulty experienced in detection of slip lines. Since the density of grown-in dislocations is high, at 2×10^6 cm^{-2}, the number of multiplication sources is also high, and slip occurs on many parallel planes. Thus the slip lines are numerous, and their surface steps small and difficult to resolve. A similar effect was seen by Patel and Chaudhuri in Ge [22].

3.3.3. Effect of surface preparation on the yield point

A sample of CMT having $x \cong 0.25$ was deformed at 120° C with a strain rate of 1.25×10^{-4} sec^{-1}, after all of its faces had been lapped on coarse (600 grade) carborundum grit. The stress–strain curve obtained is shown in Fig. 14. Also shown is a comparable stress–strain curve for a chemically polished sample. It is clear that the procedure of lapping drastically reduces the yield relaxation phenomenon. It seems probable, in the light of the results of the previous section, that this is due to the high density of fresh dislocations introduced by lapping.

Bell and Bonfield [21], in their work on Ge, found that the surface preparation had little effect on the deformation characteristics. The apparent difference for CMT arises, undoubtedly, from the difference in the volume fraction of damage introduced in the CMT and Ge tests, Firstly, in the Ge samples of Bell and Bonfield, the ratio of the surface area to the volume of the specimen gauge

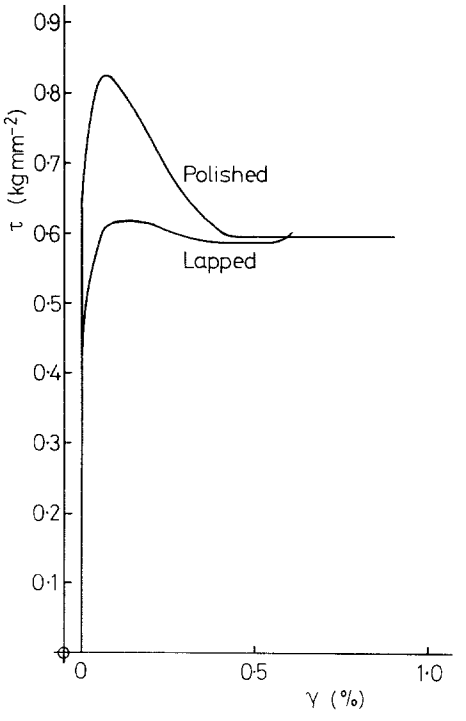

Figure 14 Stress–strain curves for ⟨1 2 3⟩ CMT samples bent in lapped and polished conditions. $T = 110°$ C $\dot{\gamma} = 1.3 \times 10^{-4}$ sec^{-1}, $x = 0.25$.

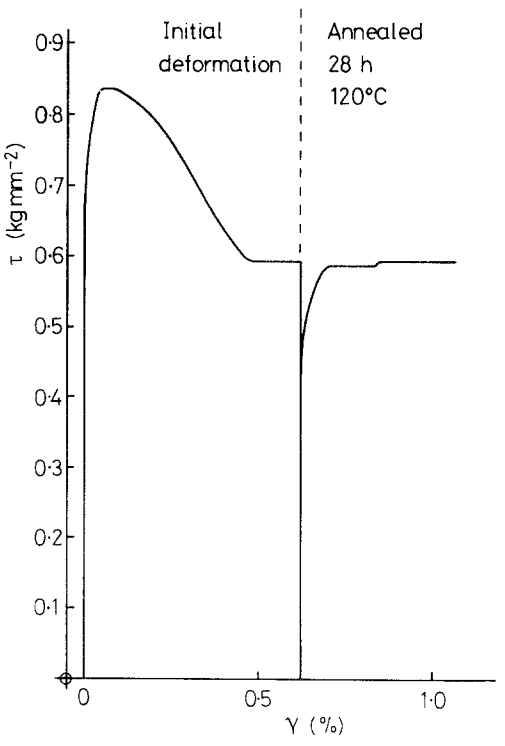

Figure 15 Stress–strain curves for ⟨1 2 3⟩ CMT ($x = 0.26$) before and after 28 h anneal in air at 120° C. $T = 120°$ C, $\dot{\gamma} = 1.3 \times 10^{-4}$ sec^{-1}.

length was 1 to 2 mm^{-1}, whereas in the present CMT samples, this ratio is about 6 mm^{-1}. Secondly, as the results of the earlier sections have demonstrated, CMT is much more susceptible to damage at room temperature than is Ge, so the depth of damage introduced in CMT should be correspondingly greater. The result of these factors is that the volume fraction of damage is relatively greater than in the CMT samples. Furthermore, in bending, deformation begins at the surface, so the surface would be expected to have a greater influence on the yield phenomenon than in the tensile test, which was the technique used by Bell and Bonfield.

3.3.4. Search for an impurity pinning effect

The experiments described in the previous sections indicated that the yield process in CMT is associated with a large multiplication of dislocations. However, it is not clear whether it is this multiplication itself which causes the yield relaxation [23], or that the effect arises from unpinning of dislocations from impurity atmospheres [28].

If the yielding process in CMT is associated with impurity pinning, then the yield point should be recoverable in a deformed sample by an appropriate annealing process, which would restore the atmospheres. (It is interesting to speculate on the nature of the "impurities". They might be foreign atoms (as for C in Fe) or alternatively, they might be intrinsic point defects; for example, segregation of vacancies to dislocation lines would cause climb, giving rise to subsequent non-conservative motion and a dragging effect).

To study this possibility, a sample was deformed into the zero work hardening region at 120° C, and a strain rate of 1.25×10^{-4} sec^{-1}, the test arrested, and the sample unloaded.

The upper knife edges were raised, so no load rested on the test-piece. It was then annealed at 120° C for 28 h. As described in the Appendix, this time should be sufficient for even the slowest diffusing species in CMT to segregate to the dislocations, forming a pinning atmosphere.

After the annealing period, the sample was retested under the original conditions ($T = 120°$ C, $\dot{\gamma} = 1.25 \times 10^{-4}$ sec^{-1}). The resulting stress–strain curve is shown in Fig. 15. No recovery of the yield point is observed as a result of the anneal, and the flow stress is unaltered. A second sample was

annealed for 28 h prior to any deformation; no effect of the anneal was observed on the subsequent behaviour in the bend test. Chemical etching experiments revealed no effect of the annealing treatment on the dislocation structure of either deformed or undeformed samples.

Similar results were obtained by Bell and Bonfield [21] in their work on Ge. They observed no return of the yield point unless the annealing temperature was sufficiently high, and the time sufficiently long, for recovery processes to cause a decrease in the dislocation density. This clearly implies that the yield phenomenon is directly related to the dislocation density, not to impurity segregation.

3.3.5. The yielding mechanism in CMT

We may summarize the foregoing results in the following way:

1. Chemical etching has shown that the grown-in dislocations do not appear to glide freely; rather large densities of fresh dislocations are introduced during yield.

2. The introduction of fresh dislocations by prior deformation or surface damage causes the yield point to disappear.

3. The yield point is not recovered after annealing indicating that it is not a result of the sudden release of dislocations from impurity atmospheres; the mechanism proposed by Cottrell [28] for the yield in steel.

4. The results of the strain-rate change tests showed that the value of the velocity–stress exponent, m in CMT is low (~ 2). The strain rate, $\dot{\gamma}$ is related to the mobile dislocation density, ρ_m, the Burgers' vector $\mathbf{b}$ of the dislocations and their velocity v by:

$$\dot{\gamma} = \rho_m \mathbf{b} v$$

Therefore, at constant $\dot{\gamma}$

$$v \propto \frac{1}{\rho_m}$$

and since

$$v \propto \tau^m$$

we have:

$$\tau^m \propto \frac{1}{\rho_m}$$

Since m is low in CMT, the stress τ required to maintain the stress rate $\dot{\gamma}$ is very sensitive to changes in ρ_m. Hence the stress relaxation during yield is a direct result of the observed increase in dislocation density. This is the Johnston–Gilman yielding mechanism [23].

It is suggested then, that yielding in CMT occurs by the Johnston–Gilman mechanism, in common with other semiconductors [22]. The yielding may be visualized as follows.

The undeformed crystal contains grown-in dislocations which, as a result of the complex interactions occurring during the growth process. are unable to glide freely under an applied stress. However, during the early stages of yield, they act as sources for fresh glissile dislocations. The resulting increase in the density of mobile dislocations produces a decrease in the stress required to maintain the constant strain rate, in accordance with $\tau^m \propto 1/\rho_m$. This is the yield relaxation. Following this, the narrow bands of slip generated at the sources spread laterally by cross-slip processes [19] to fill the gauge length. In the present experiment it is not clear whether the observed constant stress region which follows the lower yield point is caused by the spreading of these slip bands, or whether it results from the propagation of the yield front towards the neutral plane of the sample, as discussed in Section 3.3.2.

It is probably reasonable to assume that this mechanism also operates in HgTe. In both HgTe and CMT it was observed that the magnitude of the yield relaxation diminished dramatically with increasing temperature. This may now be understood, in terms of the yielding mechanism. The Johnston–Gilman model depends on the fact that the few mobile dislocations present prior to yield are unable to glide at a high enough velocity to sustain the strain rate unless the imposed stress is very high. They therefore multiply, and their required mean velocity decreases. However, as the temperature increases, they become more mobile, as v increases according to $v \propto \exp(-E/kT)$. Therefore, the number of dislocations necessary to sustain the strain rate decreases, so that the degree of multiplication, and consequently the magnitude of the stress relaxation at yield, diminishes.

3.4. The mechanism of plastic flow in CMT

In Section 3.2.3, the value of m was estimated for CMT as 2, which is similar to the values observed in the elemental and III–V semiconductors (e.g. InSb, $m = 2.2$ [19]). This implies that, in common with these materials dislocation motion in CMT may be controlled by the Peierls intrinsic lattice resistance.

A parameter which is useful in characterising the mechanism of thermally activated deformation is the activation volume, V^* [27]. This represents the effective size of obstacles in the glide plane which the dislocations must surmount by thermal activation. It is defined as the product $l\mathbf{b}\Delta R$, where l is the length of dislocation line between obstacles, $\mathbf{b}$ is the Burgers' vector and ΔR the distance along the slip plane between obstacles. Hence, for the Peierls mechanism, the obstacles are the lattice planes, so l and ΔR are of the order of atomic dimensions, so V^* is in the range $1-20\mathbf{b}^3$.

V^* may be calculated from strain-rate change data [27] using the relation:

$$V^* \cong kT\left(\frac{l\dot{n}\gamma_2 - l\dot{n}\gamma_1}{\tau_2 - \tau_1}\right)T$$

where $\dot{\gamma}_1$ is the base strain rate, $\dot{\gamma}_2$ the increased strain rate, τ_1 and τ_2 are the respective flow stresses. Hence, using the data of Section 3.2.3, values of V^* have been calculated for CMT. The results are given in Table II in units of $\mathbf{b}^3$, which for CMT is about $10^{-28}\,m^3$.

The validity of this method of estimating V^* depends, as for the measurements of m, on the internal structure of the crystal remaining constant during the zero work hardening region, where the strain-rate changes are made. In fact, the etching results have shown that the crystal is gradually flooded with dislocations during this region. Furthermore, it is possible that the dislocation density may change during a strain rate increment. However, as described earlier, the flow stress difference, $\tau_2 - \tau_1$, for a given $\dot{\gamma}_2$, is constant throughout the zero work hardening region. This means that, in the present case, changes in ρ_m must have a negligible influence on V^*, implying that V^* is not significantly influenced by dislocation–dislocation interactions in CMT.

TABLE II Activation volumes (V^*) for CMT calculated from strain rate change data using $\dot{\gamma}_2/\dot{\gamma}_1 = 5$. Units are $\mathbf{b}^3$

Composition, x	Temperature, T (° C)	V^*
0.30	21	4
0.24	20	7
0.19	20	7
0.23	42	9
0.25	103	19
0.29	140	36
0.24	143	18
0.19	144	45
0.28	196	88

The values of V^* obtained for CMT are of the order $1-10\mathbf{b}^3$, which in conjunction with the low value for m, strongly suggests that deformation is controlled by the Peierls process. The fact that V^* is independent of strain further supports this mechanism [27].

As with the measurements of m, existing data on V^* for CMT and CdTe show considerable variations. Kurilo *et al.* [4] measured V^* for CdTe, HgTe and CMT from microhardness tests, obtaining values of less than $10\mathbf{b}^3$, consistent with the present results. However, the complex stress distribution in these tests throws some doubt on their validity. Detailed data from bulk mechanical tests are available only for CdTe, and considerable variations are seen in values from the different testing techniques.

In general, V^* is observed to be strain independent, and increases with increasing temperature, both of which trends are also seen in the present results. However, the absolute values are generally higher than those obtained in the present study. Table II shows that V^* for CMT increases from about $5\,\mathbf{b}^3$ at 293 K to $50\,\mathbf{b}^3$ at 465 K. Using stress relaxation, Maeda *et al.* [2] observed such low values for CdTe only at temperatures of 150–200 K. Their V^* data at 300 K were around $200\,\mathbf{b}^3$. Similar results were obtained by Gutmanas *et al.* [3] using this technique. However, they found different values of V^* using different testing techniques; $150-200\,\mathbf{b}^3$ using strain-rate cycling and $60-80\,\mathbf{b}^3$ using pulse loading. Possible explanations for this were discussed earlier in the context of the measurements of m, and apply equally well to the V^* data. It was concluded that the greatest confidence should be applied to the pulse loading results, which in fact are of a similar order to the present data for CMT. This is supported further by the results of Osip'yan and Petrenko [30] who used a similar pulse loading technique to measure V^* for a number of II–VI compounds. They reported values at 295 K of $20\,\mathbf{b}^3$ for ZnSe, $25\,\mathbf{b}^3$ for ZnS and $50\,\mathbf{b}^3$ for CdS.

It is concluded, then, that the present data for CMT, in common with the bulk of the existing evidence, indicates that deformation in the tetrahedrally bonded II–VI compounds is controlled by the Peierls mechanism. The implications of this will now be examined.

Phillips [31] has drawn direct correlation between a number of physical parameters for various materials and the fractional ionic character

of their bonding. A number of authors have adapted this approach to the mechanism of plastic flow. It is believed that the highly covalent materials (e.g. Si) deform by the Peierls mechanism [19] whereas in the highly ionic materials (e.g. the alkali halides) dislocation motion is controlled by interaction with point obstacles [23]. Since the fractional ionicity of the II–VI compounds is intermediate between these extremes, the height of their Peierls barriers should be correspondingly lowered. It has been inferred (e.g. [10]) that the deformation mechanism might therefore, be controlled by the point obstacle mechanism.

However, Harrison [32] has pointed out that it is not appropriate to think in terms of a continuous range of behaviour between the covalent solids on one hand and the ionic solids on the other, because their crystal structures are different. In the tetrahedrally coordinated materials, the dominant feature is the strong directional covalent bond, which inevitably dominates many of the physical characteristics of the crystal, particularly the mechanical properties. The dislocation dynamics in the II–VI compounds resemble those of the covalent semiconductors because they too are tetrahedrally coordinated. On this model, any influence of the ionicity of the bond is a second order effect, unless it becomes so great that the tetrahedral coordination breaks down to the more close-packed six-fold coordination of the alkali halides. Thus, each structure should exhibit a certain range of V^* values as the bonding character varies, but which are more a characteristic of the crystal structure itself than of the ionicity. Certainly, this argument is supported by the bulk of the data on the II–VI compounds, including our own.

If the Peierls process controls the deformation in CMT then the activation energy for dislocation motion, E, calculated in Section 3.2.4 to be 0.6 eV for a composition of $x = 0.2$, is equal to the double kink formation energy [19]. Calculated values of this energy for group IV semiconductors are 1 to 2 eV. Hence it is clear that the height of the Peierls barriers does indeed decrease with increasing ionicity, as expected.

It is now well established that deformation in many II–VI compounds is strongly influenced by illumination. This is termed the photoplastic effect (PPE) [9]. Petrenko and Whitworth [33] have shown that the same deformation mechanism operates in both light and dark. Therefore. if we accept that dislocation motion in these materials is controlled by the Peierls barriers, then any theory of the PPE must be based on some modification of the intrinsic lattice resistance by illumination (e.g. that of Osip'yan and Petrenko [34]). This is further reinforced by the recent observation by Alexander [35] that, under appropriate conditions, Si exhibits a marked PPE. Likewise we are forced to reject those theories whose basis is interaction between dislocations and localised point obstacles (e.g. that of Nakagawa *et al.* [36]), since such a mechanism would give values of V^* at least an order of magnitude greater than those observed.

4. Conclusions

1. Four-point bend tests conducted on HgTe single crystals having ⟨1 2 3⟩ long axes at a glide strain rate of the order of 10^{-4} sec^{-1} and temperatures between −11 and +84° C give, at low temperatures, a stress-strain curve showing a marked yield relaxation followed by a region of zero work hardening which extends to 2 or 3% plastic strain. As the temperature is raised, the magnitude of the yield relaxation diminishes, eventually disappearing at 84° C.

2. At a strain rate of 10^{-4} sec^{-1}, the lower yield stress τ_{1y} for HgTe decreases rapidly with increasing temperature from 1.4 kg mm^{-2} at 11° C to 0.3 kg mm^{-2} at 84° C. The results obey the relation $\tau_{1y} \propto \exp(Q/kT)$ where $Q \cong 0.11$ eV.

3. At a given temperature and strain rate, the yield stress for HgTe is independent of the crystallographic sense of bending, suggesting that the same type of dislocation controls the bending in both senses. This is likely to be the screw dislocation.

4. The glide stress–glide strain curves for CMT single crystals having ⟨1 2 3⟩ long axes, and compositions in the range $0.18 < x < 0.30$, measured in four-point bending at 20° C and a glide strain rate of the order of 10^{-4} sec^{-1}, display a yield relaxation followed by a region of zero work hardening, as observed for <1 2 3> oriented HgTe samples. The magnitude of the yield stress diminishes as temperature increases, although it does not disappear, even at the highest temperature used (195° C). The measured upper and lower yield stresses for CMT ($x = 0.19$) at 20° C are 2.9 and 2.5 kg mm^{-2} respectively, falling to 0.5 and 0.4 kg mm^{-2} at 140° C.

5. The upper and lower yield stresses for CMT

measured at a strain rate of 10^{-4} sec^{-1} and temperatures of 20 and 140° C, increase markedly with increasing CdTe content, in the range $0 < x < 0.30$, in qualitative agreement with earlier hardness results [7]. The hardening rate in the composition range below $x = 0.2$ may be approximately described by the solution hardening theory due to Mott and Nabarro [24].

6. The upper and lower yield stresses, measured as a function of temperature on samples of different composition, and normalised to a composition of $x = 0.20$, obey relations of the form $\tau \propto \exp(Q/kT)$ with $Q_{uy} = 0.15$ eV and $Q_{1y} = 0.16$ eV.

7. At a fixed temperature (in the range 40 to 192° C) the post-yield flow stress, τ_f, for CMT having x around 0.25 increases with increasing strain rate, $\dot{\gamma}$ in accordance with $\tau_f \propto \dot{\gamma}^{1/n}$ where n is about 4.

8. The behaviour of the lower yield stress of CMT ($0.20 < x < 0.25$) in the temperature range 20 to 195° C at strain rates between 1.25×10^{-4} sec^{-1} and 6×10^{-3} sec^{-1} is described by the relation $\tau_{1y} \propto \dot{\gamma}^{1/4} \exp[0.16(\text{eV})/kT]$. Using the model of Haasen [25], it may be inferred that, for CMT ($x \cong 0.2$) the velocity-stress exponent $m \cong 2$ and the activation energy for dislocation motion $E \cong 0.6$ eV, so that the velocity $v \propto \tau^2 \exp[-0.6(\text{eV})/kT]$.

9. Yielding in CMT is associated with a large increase in the density of mobile dislocations. The magnitude of the yield relaxation is diminished dramatically if fresh dislocations are introduced by damage. Pinning of dislocations by impurities appears to play no part in the yield phenomenon. These facts, combined with the low value of m, lead to the suggestion that the yield mechanism is similar to that proposed by Johnston and Gilman [23] for LiF. It appears that the grown-in dislocations do not themselves glide, but rather, act as sources for fresh dislocations during yield.

10. Values of the activation volume, V^*, calculated from strain rate change tests on ⟨123⟩ oriented CMT crystals ($0.18 < x < 0.30$) lie in the range 5 to 50 $\mathbf{b}^3$ at temperatures between 40 and 140° C. These results suggest that deformation in CMT is controlled by the surmounting of Peierls barriers, in common with the other II–VI compounds.

11. The way in which deformation spreads in the bend test may explain the existence of the post-yield zero work hardening region.

Acknowledgements

The authors are indebted to colleagues at Mullard, Southampton, for performing the infra-red transmission measurements, and to the colleagues at RSRE, Malvern, where the bend jig was constructed. The invaluable advice of Professors W. D. Nix and W. A. Harrison of Stanford University, California is gratefully acknowledged. Thanks are due to the Science and Engineering Research Council for financial support and to Professor S. P. Hutton for provision of laboratory facilities at Southampton University.

Appendix

Estimation of the annealing time necessary to restore solute atmospheres to dislocations in a deformed CMT crystal

Consider an undeformed sample of CMT, in which we assume all the dislocations to be pinned by impurity atoms of some sort. Let this now be deformed, so that all the dislocations are unpinned from these atmospheres and glide until the load is removed. The impurity atoms still lie at the original sites of the dislocation lines. In order for them once more to pin the dislocations, they must diffuse to the new dislocation sites. The maximum distance, L, that an impurity atom must diffuse is equal to one half of the mean dislocation spacing in the deformed material. For a dislocation density of 3×10^7 cm^{-2} the mean dislocation spacing is $1/(3 \times 10^7)^{1/2}$ cm, giving L as $1/2(3 \times 10^7)^{1/2}$ cm.

If we now know the diffusion coefficient, D, of the pinning impurity at the annealing temperature, we may estimate the necessary annealing time, t, from the well-established approximation [37] $L = (Dt)^{1/2}$ since we do not know which species might cause pinning, it is necessary to allow time for the slowest possible species to segregate to the dislocations. At about 120° C, the lowest probable value of D in CMT is of the order of 10^{-13} cm^{-2} sec^{-1} [38]. Hence

$$t = \frac{L^2}{D}$$

$$\cong 10^5 \text{ secs}$$

$$\cong 28 \text{ h}$$

Therefore an anneal of 28 h at 120° C should restore any solute atmospheres to the dislocation lines. If solute pinning controls the yield in CMT, this treatment should, therefore, also restore the yield point in the deformed material.

References

1. E. L. HALL and J. B. VAN DER SANDE, *J. Amer. Ceram. Soc.* **61** (1978) 417.
2. K. MAEDA, K. NAKAGAWA and S. TAKEUCHI, *Phys. Status Solidi (a)* **48** (1978) 587.
3. E. Y. GUTMANAS, N. TRAVITSKY, U. PLITT and P. HAASEN, *Scripta Metall.* **13** (1979) 293.
4. I. V. KURILO, I. M. SPITKOVSKII and A. D. SHNEIDER, *Izv. VUZ Fizika* **9** (1974) 130.
5. B. P. KOMAN and M. V. PASHOVSKII, *Ukr. Fizika Zh.* **23** (1978) 58.
6. S. COLE *J. Mater. Sci.* **15** (1980) 2591.
7. S. COLE, M. BROWN and A. F. W. WILLOUGHBY, *Ibid.* **17** (1982) 2061.
8. S. COLE, A. F. W. WILLOUGHBY and M. BROWN, *J. Cryst. Growth* **59** (1982) 370.
9. YU, A. OSIP'YAN and I. B. SAVCHENKO, *Sov. Phys. JETP Lett.* **7** (1968) 100.
10. E. Y. GUTMANAS, P. HAASEN and N. TRAVITSKY, *Phys. Status Solidi* (a) **51** (1979) 435.
11. E. L. POLISAR, N. M. BOINIKH, G. V. INDENBAUM, A. V. VANYUKOV and V. P. SCHASTLIVII, *Izv VUZ Fizika* **6** (1968) 81.
12. M. BROWN and A. F. W. WILLOUGHBY, *J. De Physique Colloque C6* **40** (1979) 151.
13. P. F. FEWSTER, S. COLE, A. F. W. WILLOUGHBY and M. BROWN, *J. Appl. Phys.* **52** (1981) 4568.
14. B. E. BARTLETT, P. CAPPER, J. E. HARRIS and M. J. T. QUELCH, *J. Cryst. Growth* **46** (1979) 623.
15. D. LONG and J. L. SCHMIT in "Semiconductors and Semimetals", Vol 5, edited by R. K. Willardson and A. C. Beer (Academic Press, New York, 1970).
16. A. A. BRUNEAU and P. L. PRATT, *Philos. Mag.* **7** (1962) 187.
17. American Society for Metals, "Metals Handbook", Vol. 1 8th Edition.
18. K. SUMINO and H. SHIMIZU, *Philos. Mag.* **32** (1975) 123 and 143.
19. H. ALEXANDER and P. HAASEN, *Solid State Phys.* **22** (1968) 27.
20. R. L. BELL and A. F. W. WILLOUGHBY, *J. Mater. Sci.* **5** (1970) 198.
21. R. L. BELL and W. BONFIELD, *Philos. Mag.* **9** (1964) 9.
22. J. R. PATEL and A. R. CHAUDHURI, *J. Appl. Phys.* **34** (1963) 2788.
23. W. G. JOHNSTON and J. J. GILMAN, *ibid.* **30** (1959) 129.
24. N. F. MOTT and F. R. N. NABARRO, "Report of a Conference on Strength of Solids", (The Physical Society, London) p.1.
25. P. HAASEN, discussed in [19].
26. L. CARLSSON and C. N. AHLQUIST, *J. Appl. Phys.* **45** (1972) 2529.
27. A. G. EVANS and R. D. RAWLINGS, *Phys. Staus Solidi* **34** (1969) 9.
28. A. H. COTTRELL in"Report of a Conference on Strength of Solids" Bristol (1947) (The Physical Society, London) p.30.
29. T. C. HARMAN in "Physics and Chemistry of II–VI Compounds", edited by M. Aven and J. S. Premer (North Holland Publishing Company, Amsterdam, 1967) p.785.
30. YU. A. OSIP'YAN and V. F. PETRENKO, *Sov. Phys. JETP* **48** (1978) 147.
31. J. C PHILLIPS, "Bonds and Bands in Semiconductors", (Academic Press, New York, 1973).
32. W. A. HARRISON, private communication.
33. V. F. PETRENKO and R. W. WHITWORTH, *Philos. Mag.* **A41** (1980) 681.
34. YU. A. OSIP'YAN and V. F. PETRENKO, *Sov. Phys. JETP* **42** (1975) 695.
35. K. H. KUSTERS and H. ALEXANDER, *Physica B & C* **116B+C** (1983) 594.
36. K. NAKAGAWA, J. MAEDA and S. TAKEUCHI, *J. Phys. Soc. Japan* **50** (1981) 3040.
37. W. J. MOORE, "Physical Chemistry" (Longman, London, 1972) p.163.
38. M. BROWN and A. F. W. WILLOUGHBY, *J. Cryst. Growth* **59** (1982) 27.

Received 28 February
and accepted 13 March 1984